Selective Nanovector Mediated Treatment of Activated Proinflammatory Microglia/ Macrophages in Spinal Cord Injury

Simonetta Papa,[†,¶] Filippo Rossi,[‡,¶] Raffaele Ferrari,[‡] Alessandro Mariani,[§] Massimiliano De Paola,[§] Ilaria Caron,[†] Fabio Fiordaliso,[⊥] Cinzia Bisighini,[⊥] Eliana Sammali,[†] Claudio Colombo,[‡] Marco Gobbi,[∥] Mara Canovi,[∥] Jacopo Lucchetti,[∥] Marco Peviani,[#] Massimo Morbidelli,[◆] Gianluigi Forloni,[†] Giuseppe Perale,[‡,▽,⊗] Davide Moscatelli,[‡] and Pietro Veglianese[†,*]

[†]Dipartimento di Neuroscienze, IRCCS Istituto di Ricerche Farmacologiche "Mario Negri", via La Masa 19, 20156 Milan, Italy, [‡]Dipartimento di Chimica, Materiali e Ingegneria Chimica "Giulio Natta", Politecnico di Milano, via Mancinelli 7, 20131 Milan, Italy, [§]Dipartimento di Ambiente e Salute, IRCCS Istituto di Ricerche Farmacologiche "Mario Negri", via La Masa 19, 20156 Milan, Italy, [⊥]Dipartimento di Ricerca Cardiovascolare, IRCCS Istituto di Ricerche Farmacologiche "Mario Negri", via La Masa 19, 20156 Milan, Italy, [∥]Dipartimento di Biochimica e Farmacologia Molecolare, IRCCS Istituto di Ricerche Farmacologiche "Mario Negri", via La Masa 19, 20156 Milan, Italy, [#]Dipartimento di Biologia e Biotecnologie "L. Spallanzani", Università di Pavia, via Ferrata, 9, 27100 Pavia, Italy, [▽]Department of Innovative Technologies, University of Applied Sciences and Arts of Southern Switzerland, SUPSI, via Cantonale, CH-6928 Manno, Switzerland, [⊗]Swiss Institute for Regenerative Medicine, CH-6807 Taverne, Switzerland, and [◆]Institute for Chemical and Bioengineering, ETH Zurich, Campus Hoenggerberg, HCI F125, Wolfgang Pauli Str. 10, 8093 Zurich, Switzerland. [¶]S. Papa and F. Rossi contributed equally to this work.

ABSTRACT

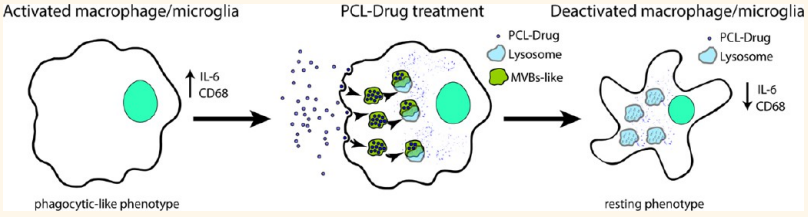

Much evidence shows that acute and chronic inflammation in spinal cord injury (SCI), characterized by immune cell infiltration and release of inflammatory mediators, is implicated in development of the secondary injury phase that occurs after spinal cord trauma and in the worsening of damage. Activation of microglia/macrophages and the associated inflammatory response appears to be a self-propelling mechanism that leads to progressive neurodegeneration and development of persisting pain state. Recent advances in polymer science have provided a huge amount of innovations leading to increased interest for polymeric nanoparticles (NPs) as drug delivery tools to treat SCI. In this study, we tested and evaluated *in vitro* and *in vivo* a new drug delivery nanocarrier: minocycline loaded in NPs composed by a polymer based on poly-ε-caprolactone and polyethylene glycol. These NPs are able to selectively target and modulate, specifically, the activated proinflammatory microglia/macrophages in subacute progression of the secondary injury in SCI mouse model. After minocycline-NPs treatment, we demonstrate a reduced activation and proliferation of microglia/macrophages around the lesion site and a reduction of cells with round shape phagocytic-like phenotype in favor of a more arborized resting-like phenotype with low CD68 staining. Treatment here proposed limits, up to 15 days tested, the proinflammatory stimulus associated with microglia/macrophage activation. This was demonstrated by reduced expression of proinflammatory cytokine IL-6 and persistent reduced expression of CD68 in traumatized site. The nanocarrier drug delivery tool developed here shows potential advantages over the conventionally administered anti-inflammatory therapy, maximizing therapeutic efficiency and reducing side effects.

KEYWORDS: nanoparticle · spinal cord injury · minocycline · microglia · inflammation · neurodegeneration · drug delivery

The spinal cord trauma results from a *primary injury* due to contusive, compressive, or stretch insults followed by a multifactorial *secondary injury* that worsens the clinical outcomes.[1,2] This leads to motor dysfunction below the level of lesion, as well as development of chronic pain syndrome. Among the physiopathological mechanisms involved in the progression of spinal cord injury, inflammation is one of the most relevant. In fact, much evidence shows that acute inflammation, characterized by microglia activation and immune cell infiltration (lymphocytes, neutrophils, and macrophages) and by the release of inflammatory mediators (cytokine and chemokines), results in spreading and exacerbation of tissue injury, eventually leading to chronicity and persistent pain

* Address correspondence to pietro.veglianese@marionegri.it.

Received for review July 15, 2013 and accepted October 5, 2013.

Published online October 18, 2013
10.1021/nn4036014

© 2013 American Chemical Society

syndrome.[3,4] Accumulating evidence points to microglia/macrophages as key cellular players crucially involved in the inflammatory events.[3,5] Indeed, microglial cells rapidly respond to CNS traumatic insults by adopting an activated phenotype (amoeboid or phagocytic shape). Activated microglia/macrophages dominate sites of SCI soon after the trauma and persist in the tissue for several weeks, promoting both injury and repair. These divergent effects are associated with distinct microglia/macrophage phenotypes, *i.e.*, "classically activated" proinflammatory (M1) or "alternatively activated" anti-inflammatory (M2) cells. Interestingly, it has been shown that M1 response is rapidly induced and then maintained at sites of traumatic spinal cord injury in the subacute and chronic phase, whereas M2 response is transient and limited to the subacute phase of the trauma.[6,7] Prolonged microglia/macrophage activated phenotype sustains a long-term release of different proinflammatory mediators such as proinflammatory cytokines (IL-1β, IL-6, and TNFα), chemokines, nitric oxide, and superoxide free radicals.[6,8,9] This suggests that a long-term activation of microglia/macrophages and the associated inflammatory response could be a self-propelling mechanism of progressive neurodegeneration and chronic pain. In this view, a pharmacological approach, specifically tailored to modulate microglia/macrophage activation, would provide better chances to interfere with microglia/macrophage-related inflammatory events. This approach would possibly lead to improve the clinical outcomes in the therapy of *secondary injury*, an aspect of SCI therapy that is still challenging in clinical practice.

Growing interest in the improvement of *in situ* drug delivery system to treat SCI was demonstrated in the last years.[10−13] Recent advances in polymer science have provided a huge amount of innovations, underlining the increasing importance of polymeric nanoparticles (NPs) in biomedical applications.[14,15] Recently, new evidence *in vitro* and *in vivo* suggests that NPs are selectively internalized by macrophage cells, because of their specific endocytic/fagocytic activity of foreign bodies.[16−18] It is known that microglia/macrophages can assume phagocytic activity after traumatic stimuli,[3,5] and this property makes NPs an excellent tool for drug targeting. This represents an attractive strategy to exploit macrophagic cells using NPs as Trojan horses for targeted drug delivery.[16] This approach would possibly improve drug efficacy and reduce potential side effects associated with systemic treatments.

Specifically, in this work we developed and characterized a new selective delivery tool: biodegradable polymeric NPs, of 100 nm in size; such NPs are obtained through a two-step process, both solvent-free, and possess a peculiar comb-like structure, where a poly-(2-hydroxy-ethyl methacrylate) backbone is grafted with PCL and PEG chains both controllable in terms of length and composition. Then, PEG chains are covalently linked to the NPs, ensuring the stability, and the low molecular weight of them (up to 2000 Da) allows tuning the degradation rate of the NPs from two days to one month in biological conditions (cell medium, 37 °C).[19] These NPs present unique properties such as biocompatibility and the possibility to sustain the release of drugs. Moreover, their high versatility allows control of their degradation rates depending on medical needs. We provide evidence that these polymeric NPs can supply optimized specific targeting of activated microglia/macrophages, *in vivo*, and can release an anti-inflammatory drug (minocycline) *in situ*. This represents a proof of concept of the possibility to exploit this new drug delivery tool for specifically modulating activated microglia/macrophages and the associated proinflammatory events.

RESULTS

PCL-Based NP Synthesis and Characterization. In this study we characterized fluorescent poly-ε-caprolactone (PCL)-based NPs, conjugated with Rhodamine B (RhB) and synthesized by emulsion-free radical polymerization. Their comb-like structure is constituted of a poly-(2-hydroxyethyl methacrylate) backbone, hereafter called poly(HEMA), in which each HEMA unit is grafted with a PCL chain composed of a controllable number of CL units. These NPs, because of their peculiar structure, offer the possibility to tune the polymer hydrophobicity and the NP degradation rate, by acting on the PCL chain length. Their high biocompatibility due to the single components used, along with the possibility to tune the degradation profiles and the drug release, are the main advantages of this class of NPs. In addition, the emulsion-free radical polymerization ensures a very homogeneous and narrow particle size distribution and an easy control over final average particle size as well as an easy PEGylation of the NPs aimed to increase the NP biocompatibility. The degradation pathway of these comb-like NPs occurs through a swelling mechanism, leading to a full degradation of PCL side chains leaving the polyHEMA backbone linked to the PEG chains.[20] Pegylated polyHEMA chains are hydrosoluble and can be easily disposed; additionally, it was demonstrated that such polymer does not undergo further degradation leading to possible nonbiocompatible products, such as ethylene glycol.[21]

The final diameter, the polydispersity index (PDI), and ζ potential of the fluorescent PEGylated PCL-based NPs, as measured through dynamic light scattering (DLS), are reported in Table 1 together with the same characteristics measured after 48 h of incubation in cell medium and after drug loading procedure, thus proving the NP stability in the condition involved in the present study. The particle size distribution, highlighting the monodispersity of the sample, is reported in Figure 1A together with the ^{1}H NMR of the copolymer (Figure 1B), which proves the PCL-PEG copolymer

TABLE 1. Characteristics of the Produced Fluorescent NPs as Measured by DLS

			post synthesis		48 h incubation with cell medium		post drug loading procedure	
material	PEGylation	size [nm]	PDI [—]	ζ-potential [mV]	size [nm]	PDI [—]	size [nm]	PDI [—-]
HEMA-CL_3	HEMA-PEG_{19}	108	0.070	−2.6	101	0.095	112	0.102
HEMA-CL_3	—	114	0.020	−22	132	0.102	—	—
MMA	HEMA-PEG_{19}	102	0.057	−3.7	101	0.061	—	—

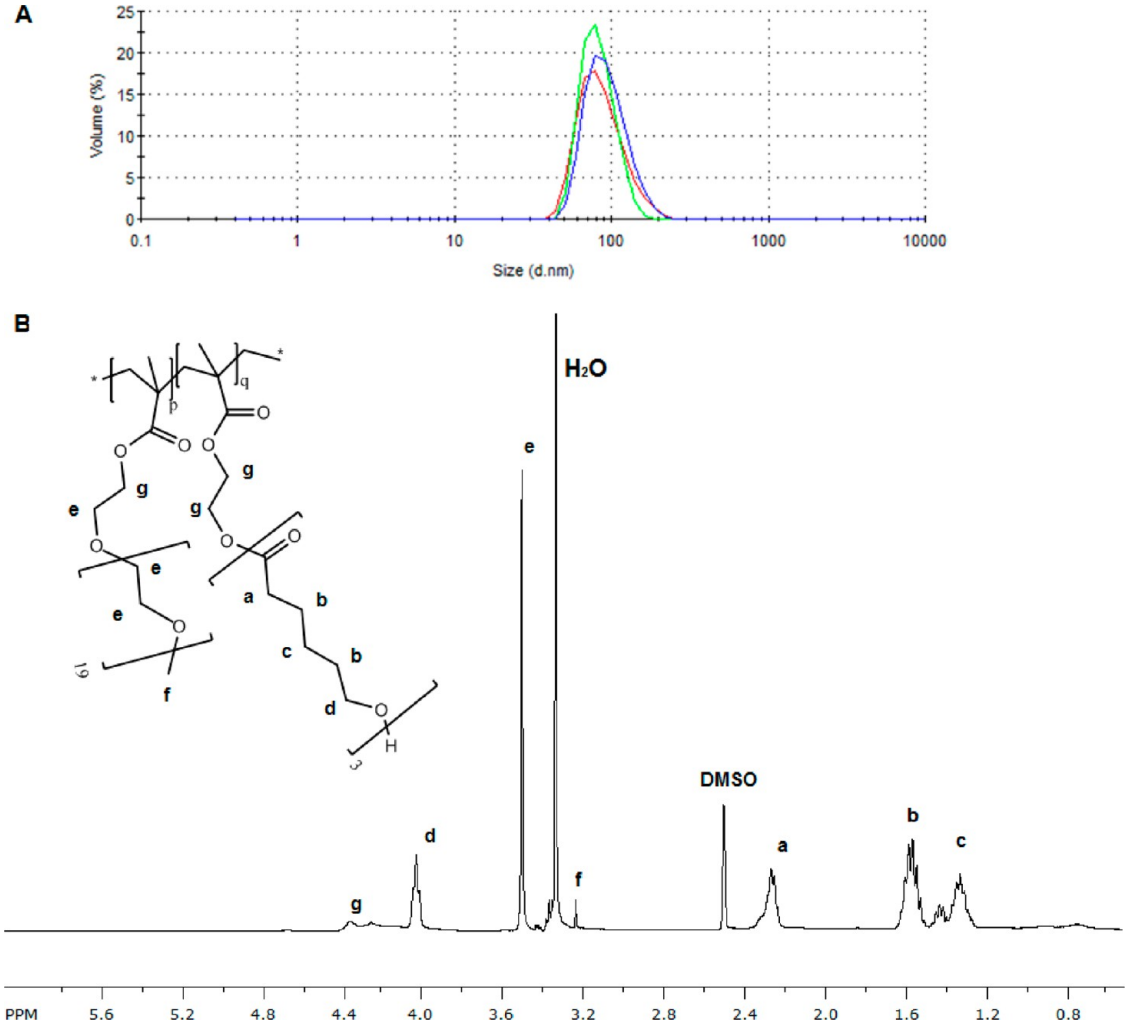

Figure 1. (A) Volume particle size distribution of the produced PCL-PEG NPs (red line), PCL NPs (blue line), and PMMA-PEG NPs (green line). (B) ^{1}H NMR of the PCL-PEG polymer constituting the NPs.

synthesis. Additionally, data for non PEGylated PCL-based NPs and PEGylated poly(methyl methacrylate)-based NPs (PMMA-PEG NPs), used during the present study, are also reported in Table 1 and Figure 1A.

Cellular Uptake Study of PCL-Based NPs and Metallic Qdot655 *in Vitro*. Primary cocultures of microglia, astrocytes, and neurons from the spinal cord of mouse embryos were used to characterize the uptake of PCL-based NPs (covalently linked to RhB to avoid dye leakage from the NPs). The uptake of biodegradable PCL-based NPs was compared to the uptake of metallic Qdot655, the latter commercially available NPs already used in a previously published paper.[17] Specific antibodies were used to detect astrocytes, microglia, and neurons (respectively stained for GFAP, CD11b and NF200). An activated phenotype was induced in microglia by treatment with LPS for 18 h. LPS is a potent activator of monocytes and macrophages and is commonly used to activate microglial cells *in vitro* and *in vivo*. Morphological changes have been verified for LPS-treated microglial cells, which showed a hypertrophic shape (amoeboid/phagocytic shape) in comparison to unstimulated microglial cells (Figure 2A). In addition, a cell viability assessment in neuroglial cultures was performed

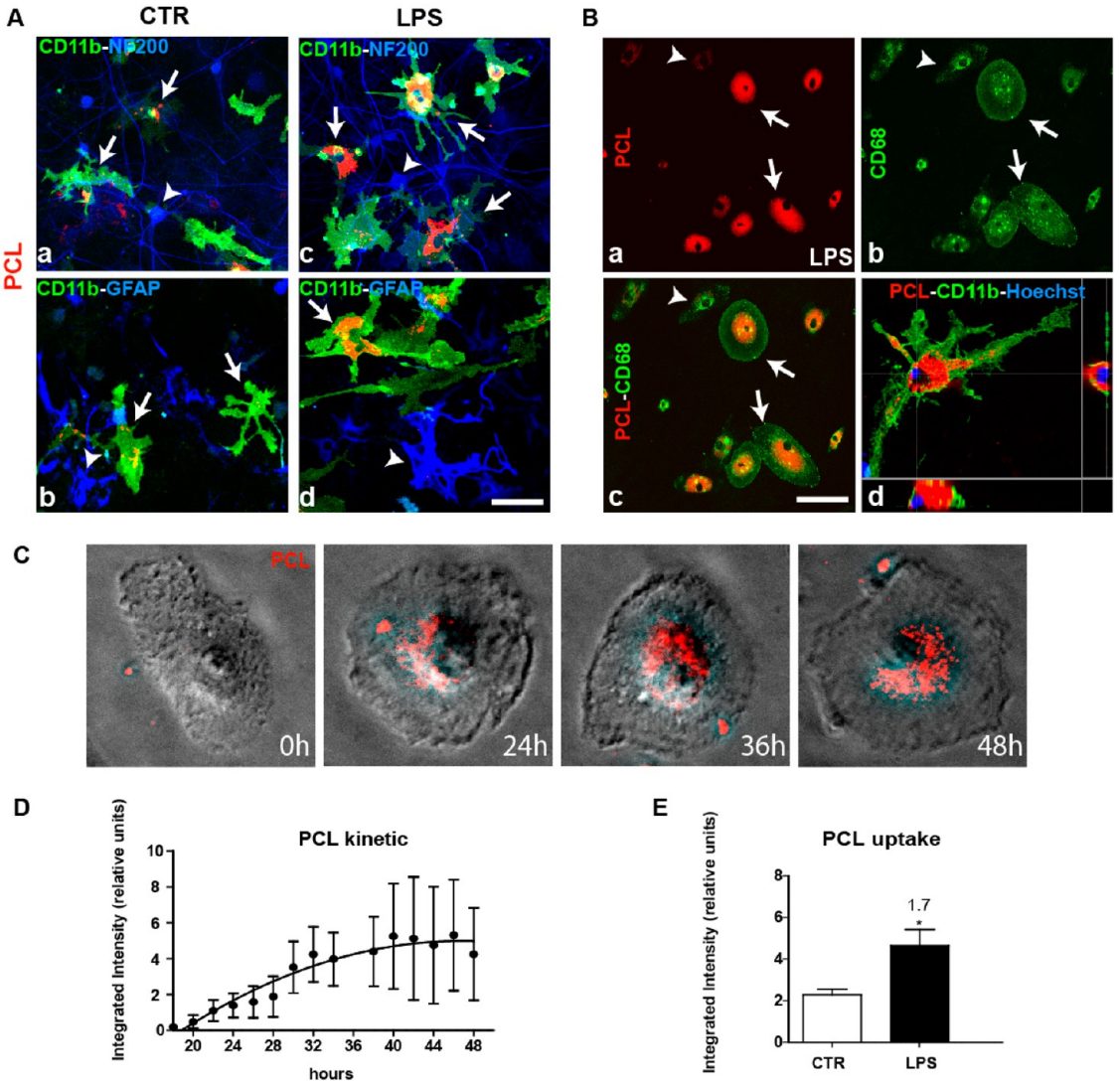

Figure 2. *In vitro* **characterization of PCL-based NP uptake and distribution. (A) Characterization of PCL-based NP uptake in primary cocultures of microglia, astrocytes and neurons. In LPS-stimulated cells (c,d), microglia show a hypertrophic shape compared to control condition (a,b), while no changes are present in neurons (a−c) and astrocytes (b−d). Accumulation of fluorescent PCL-based NPs is markedly increased in LPS-stimulated microglial cells (c,d, arrows) in comparison to control condition (a,b, arrows). No uptake is observed for both astrocytes (a,c arrowheads) and neurons (b,d arrowheads). Microglia, CD11b (green); PCL-based NPs, RhB (red); astrocytes, GFAP (blue) (b−d); neurons, NF200 (blue) (a−c). Scale bar =15 μm. (B) Microglia displaying high level of CD68 staining (b,c, arrows) show a higher internalization of PCL-based NPs compared to low CD68-positive microglia (a,b,c arrowheads). Scale bar =15 μm. (d) Orthogonal projection of confocal image stack shows the internalization of PCL-based NPs by activated ameboid microglial cells. Microglia, CD11b (green); PCL-based NPs, RhB (red); cell nuclei, Hoechst (blue). (C) Time-lapse analysis of uptake kinetics of PCL-based NPs by activated microglia. Cytosolic localization of NPs (red signal) progressively evolved in a perinuclear distribution, with a plateau reached after 48 h. (D) Quantitative evaluation of progressive PCL internalization in activated microglial cells during time lapse analysis. Data are presented as mean ± SD. (E) Uptake quantification of NPs in activated microglia (LPS) *vs* unstimulated cells (CTR) shows a significantly increased NPs internalization in LPS-stimulated cells (about 1.7-fold). Data are presented as mean ± SEM. Statistical significance: (*)p = 0.05.**

showing a lack of both morphological alteration and vitality in astrocytes, whereas 30% of neuronal death was detected. The NP uptake evaluation was performed only in healthy neuroglial cells detected as negative staining for propidium iodide (cell death marker) (Figure 2A). Analyzing both PEGylated and not PEGylated form of PCL (0.05% monomer w/v), we found that the latter showed toxicity on cocoltures, already after 3 h of incubation (data not shown). Not-PEGylated toxicity was detected as propidium iodide positive microglial cells (95−100% cell death after 48 h). Thus, only the PEGylated form was further tested and used in this study (hereafter termed just PCL-based NPs). After the exposure of unstimulated neuron/glia cocultures to NPs, a few internalized PCL-based NPs were revealed selectively in CD11b positive microglial cells (CTR, Figure 2A). On the contrary, a greater Qdot655 internalization was detected in unstimulated microglia compared to PCL-based NPs (CTR, Figure S1A, Supporting Information). Noteworthy, when we analyzed LPS-stimulated cocultures, a remarkable

increase in PCL-based NP (LPS, Figure 2A) and Qdot655 (LPS, Figure S1A, Supporting Information) uptake was detected selectively in activated microglial cells compared to unstimulated cells, showing a diffuse and intense specific signal in the cytosol. The quantification of internalized NPs in microglia revealed a great difference between unstimulated and activated microglia for both PCL (Figure 2E, 1.7 fold; CTR 2.28 ± 0.27 *vs* LPS 4.65 ± 0.77 mean integrated intensity ± SEM) and Qdots655 uptake (Figure S1B, Supporting Information, 1.4 fold; CTR 14.61 ± 0.27 *vs* LPS 20.12 ± 1.41 mean integrated intensity ± SEM). This suggests a higher selectivity for activated microglia for PCL-based NPs in respect to commercial Qdots655.

To confirm that an increase in PCL-based NP uptake selectively occurred in activated microglial cells, an immunostaining for CD68 was carried out. CD68 is a glycoprotein highly expressed when microglia/macrophages are activated. Thus, an increased CD68 staining is usually considered a specific marker of microglia/macrophage activation. Immunocytochemistry confirmed that microglia displaying higher CD68 signal in both cytosol and membrane region showed a more marked internalization of NPs (arrows, Figure 2B) compared to low level CD68-positive cells that were stained mostly in the cytosol (arrowheads, Figure 2B). Time-lapse analysis was performed to investigate the uptake kinetics of PCL-based NPs by LPS-activated microglia. We observed that PCL-based NP uptake was detectable already after 24 of treatment, reaching a plateau after 48 h of incubation (Figure 2C,D).

PCL-Based NP Internalization and Degradation *in Vitro*. To investigate the mechanisms underlying the internalization of PCL-based NPs, we tested the effect of a specific clathrin-mediated endocytosis inhibitor, chlorpromazine (CPZ), on NP uptake in activated microglial cells. LPS-stimulated microglia were pretreated with different concentrations of CPZ (30−40−50 μM) for 2 h before being exposed to the NPs. The quantification of NP uptake revealed that a significant dose-dependent inhibition of PCL uptake in activated microglia was induced by 30 (2.15 ± 0.39 mean integrated intensity ± SEM) and 40 μM (1.21 ± 0.26 mean integrated intensity ± SEM) CPZ compared to cells not treated with CPZ (LPS), used as control (4.90 ± 0.64 mean integrated intensity ± SEM) (Figure 3A,B). Differently, 50 μM CPZ showed cytotoxic effect on microglial cells (data not shown).

Further analyses using transmission electron microscopy (TEM) have been carried out to investigate the intracellular distribution of NPs after their internalization in the cytosol of microglial cells. TEM analysis confirmed the internalization of PCL-based NPs into the cytosol by activated microglial cells confined in lysosomes, probably derived from the fusion of a multivesicular body (MVB) with a primary lysosome occurring at an earlier stage (Figure 3C). In spite of a large amount of internalized and stored NPs, no morphological alterations have been detected in the fundamental organelles of the cytosol. In fact, normal ultrastructures of mitochondria, nucleus, endoplasmic reticulum, and Golgi apparatus were observed in activated microglial cells exposed to NPs, compared to untreated microglial cells (Figure 3Ca, D). Our assessment by TEM of the physical state of the NPs revealed, already at 2 days after treatment, areas of PCL-based NP debris concentration that seem still to retain the original localization in the intraluminar vesicles of MVB digested later on by the fusion with a lysosome (Figure 3C). At 6 days after treatment a complete degradation of PCL-based NPs was found, as shown by a more diffuse polymeric debris in lysosomes (Figure 3Cc,d). To further confirm the PCL-based NPs degradation by the enzymatic lysosomal activity, a lysosensor, a fluorescent pH indicator that measures the activity of acidic organelles, was used to study the lysosome function in live microglia after NPs exposure. Noteworthy, an increased lysosomal enzymatic activity, represented by an increased green signal highly colocalized with PCL RhB red signal, was detected at 6 days (Figure 3E). In order to verify our observations on PCL-based NP degradation mechanisms, we compared degradable PCL-based NPs with standard non-degradable poly(methylmethacrylate) (PMMA)-based NPs with the same diameter and PEGylation (Figure S2B, Supporting Information). PMMA-based NPs are internalized in structures with morphological characteristic of MVBs, at both 1 and 6 days after NPs exposure (Figure S2, Supporting Information). After 6 days, PMMA-based NPs still did not show any sign of degradation, resulting disperse in the cytosol of the microglial cells (Figure S2A, Supporting Information). The analysis with lysosensor revealed only some green lysosomal spots in the cytosol of microglial cells treated with PMMA-based NPs. Moreover, a lack of colocalization with NPs-RhB red signal was found, suggesting a lack of degradation of PMMA-based NPs by microglia (Figure S2C, Supporting Information). These results confirm the biodegradability and biocompatibility of PCL-based NPs, which are probably rapidly sequestered by MVBs at an early stage and then completely degraded by lysosomes. Conversely, PMMA-based NPs, after 6 days, still maintain their structure without activating the lysosomal degradative machinery.

Cell Viability and Cytokine Release after NP Internalization. To determine whether internalized PCL-based NPs are able to affect microglia viability, purified microglia cultures were exposed to NPs, and viability was determined by a colorimetric assay. PCL-based NP uptake did not affect LPS-stimulated microglial cell viability, compared to LPS-stimulated microglia not exposed to NPs, up to 6 days, as detected by MTS assay (Figure S3A, Supporting Information). Furthermore, we assessed the release of three well characterized inflammatory

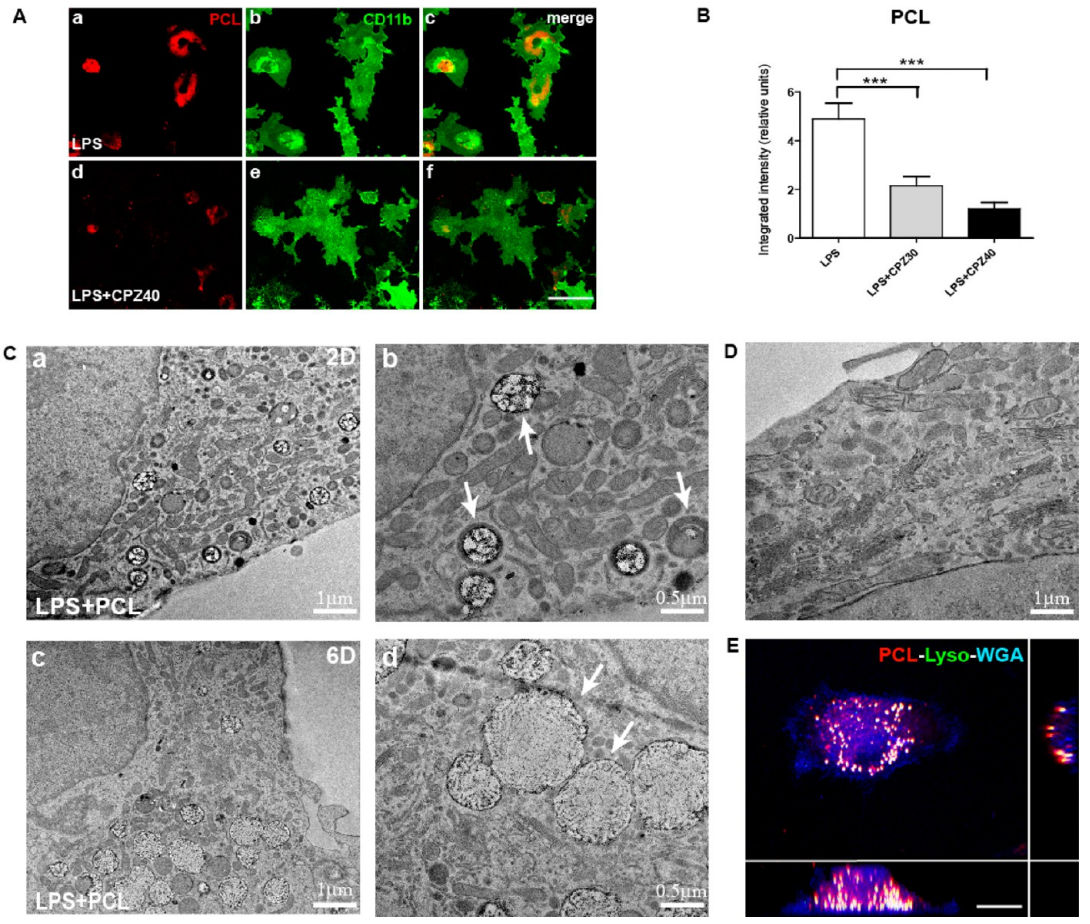

Figure 3. PCL-based NPs are endocytosed by activated microglia and degraded by lysosomes. (A) Pretreatment with Chlorpromazine (CPZ) (d−f) is able to inhibit PCL-based NP uptake by activated microglia *in vitro*. Microglia, CD11b (green); PCL-based NPs, RhB (red). Scale bar = 5 μm. (B) Quantitative analysis shows that uptake inhibition of PCL-based NPs occurs in a dose-dependent manner. (C) TEM analysis of activated microglia 2 days (a,b) or 6 days (c,d) after treatment with PCL-based NPs. NPs are visible as partially degraded in lysosomes at day 2 (a,b, arrows), while at 6 days, PCL-based NPs are completely degraded, and lysosomes contain only diffuse polymeric debris (c,d, arrows). (D) TEM analysis of untreated microglial cells. (E) PCL-based NPs are degraded by lysosomal activity. Orthogonal projection of confocal image stack shows a highly colocalized signal between PCL-based NPs and activated lysosomes (yellow); PCL-based NPs, RhB (red); lysosomes, LysoSensor (green); cell membrane, Alexa Fluor350 WGA (blue). Scale bar = 5 μm. Data are presented as mean ± SD. Statistical significance: (***)p = 0.001.

cytokines (IL-1β, IL-6, and TNFα) in neuron/glia cocultures, after treatment with NPs, in order to evaluate whether PCL-based NPs could be a further stimulus for the release of proinflammatory cytokines from LPS-stimulated cells. To better understand whether internalized polymeric NPs could affect the cytokine release from LPS-stimulated cocultures, we removed the medium after 18 h of LPS stimulation, and then cells were exposed to NPs for 48 h (when the uptake plateau was detected), detecting the subsequent release of proinflammatory cytokines from activated microglia by ELISA assay. Analyzing the medium of the cells for IL-1β, TNFα, and IL-6, we found that IL-1β and TNFα levels were below the detection limit after 48 h of NP exposure, whereas IL-6 levels were significantly increased in the medium of LPS-stimulated cocultures (148.6 ± 10.7 mean pg/mL ± SD) compared to unstimulated cells (66.8 ± 35.3 mean pg/mL ± SD) (Figure S3B, Supporting Information). However, there were no significant effects of NPs on IL-6 levels of LPs-stimulated microglial cells (169.8 ± 8.5 mean pg/mL ± SD) if compared to LPS-stimulated cells not exposed to NPs (148.6 ± 10.7 mean pg/mL ± SD).

Cellular Uptake of Polymeric PCL-Based NPs *in Vivo*. In order to evaluate and characterize the distribution of PCL-based NPs *in vivo*, an injection of hydrogel loaded with PCL-based NPs was performed within the parenchyma of mouse spinal cord, as described in Experimental Section and previously published.[22] Early after the injection, the hydrogel revealed a spherical enclosure, which physically displaced the tissue in the spinal cord, due to its *in situ* gelation. In order to investigate the inflammatory response of the nervous tissue to injury induced by the injected hydrogel, a double staining with markers for microglia (CD11b) and astrocytes (GFAP) was carried out. At 3 days postinjection (DPI), an inflammatory reaction was detected around the hydrogel, identified as a glial scar formation

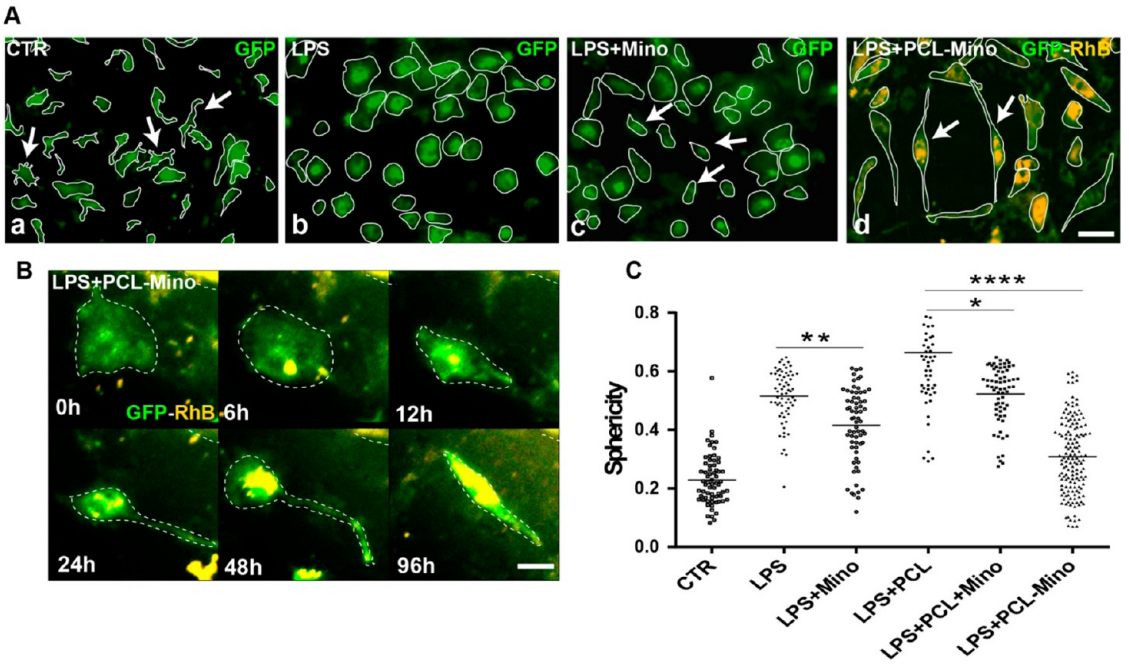

Figure 4. PCL-Mino based NP treatment of activated microglia is able to revert activation process *in vitro*. (A) In primary GFP-microglia cultures from CX3CR1 mouse embryos, LPS treated cells (b) were incubated with minocycline (LPS+Mino) (c) or with minocycline-loaded PCL-based NPs (LPS+PCL-Mino) and analyzed 96 h later (d). Scale bar = 10 μm. (B) Time lapse imaging of a single microglial cell during 96 h of treatment with LPS+PCL-Mino. At the end of the analysis, microglia show a more ramified phenotype. Microglia, GFP (green); NPs, PCL RhB (orange). Scale bar = 5 μm. (C) Evaluation of cell sphericity (index of cells activation) of microglial cells after five different treatments. Sphericity of LPS+PCL-Mino treated cells is significantly lower than either LPS+PCL or LPS+PCL+Mino treatment. Each dot represents the sphericity of a single cell. Statistical significance: (*)p = 0.01; (**)p = 0.01; (****)p = 0.0001.

composed of phagocytic/ameboid microglia and astrocytes. A distribution of PCL-based NPs was found around the injected hydrogel, revealing a selective uptake of NPs in the nearest activated-phagocytic microglial cells (see Figure 5A,B). The selective uptake by the microglial cells was confirmed detecting a lack of colocalization between NPs and GFAP/Neurotrace (Figure S4C, Supporting Information).

***In Vitro* Study of Pharmacological Activity of Minocycline Delivered by PCL-based NPs.** Minocycline was loaded in preformed PCL-based NPs by entrapment of the hydrophobic drug in partially swollen NPs (see Experimental Section for details), followed by 4 h dialysis to remove unloaded drug, as assessed by HPLC−MS/MS (Figure S4D, Supporting Information). At this dialysis time point, PCL-based NPs retain about 35% of the added minocycline, with a final loading of about 1 μg of minocycline/mg of NPs. Microglial cells *in vitro* were analyzed for their morphological criteria by comparing (I) unstimulated control cells (CTR); (II) LPS-stimulated cells (LPS); (III) LPS-stimulated cells treated with free minocycline (LPS+Mino, 0.07 μg/mL); (IV) LPS-stimulated cells subsequently exposed to PCL (LPS+PCL); (V) LPS-stimulated cells subsequently exposed to both PCL and free minocycline (LPS+PCL+Mino, 0.07 μg/mL); and (VI) LPS-stimulated cells treated with minocycline encapsulated in PCL-based NPs (LPS+PCL-Mino, 0.07 μg/mL loaded). Unstimulated microglial cells showed a small soma with some ramified processes (Figure 4Aa). Differently, LPS-stimulated microglial cells displayed a round shape typical of fully activated microglia with a macrophage phenotype (Figure 4Ab). Evaluating activated microglial cells treated for 96 h with PCL-Mino, a relevant regression toward a quiescent phenotype was found (Figure 4Ad). In fact, a reduced round shape phenotype and the reappearance of thick processes could be appreciated after PCL-Mino treatment. This was confirmed also by quantitative evaluation of the sphericity (from 0 to 1, respectively, ramified and round shape) as a morphological parameter for the evaluation of the activation state of the microglial cells. This assessment showed a significantly reduced value for LPS+PCL-Mino (0.31 ± 0.13 mean sphericity ± SD) compared to LPS+PCL (0.67 ± 0.17 mean sphericity ± SD) (Figure 4C). The regression toward a more quiescent phenotype was further demonstrated by time lapse analysis on single cells that showed a morphologically defined stepwise deactivation up to 96 h (Figure 4B). Analyzing LPS+PCL (0.67 + 0.17 mean sphericity ± SD) an increased, but not significant, sphericity was detected compared to LPS (0.52 + 0.09 mean sphericity ± SD), likely due to NP uptake (Figure 4C). A significant reduced sphericity was detected also for cells treated with LPS+Mino (0.41 ± 0.12 mean sphericity ± SD) and LPS+PCL+Mino (0.52 ± 0.10 mean sphericity ± SD) when compared

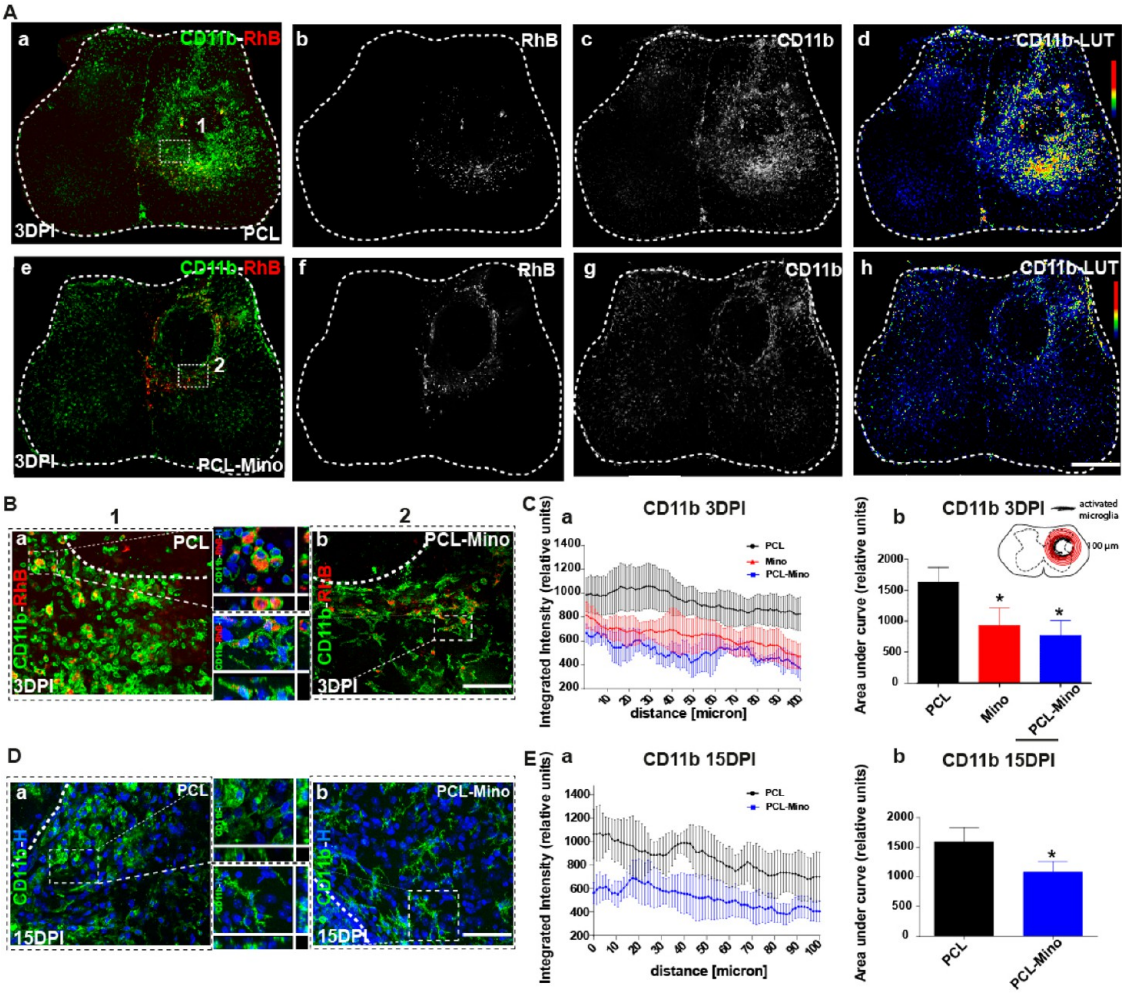

Figure 5. PCL-Mino based NP treatment of activated microglia is able to revert activation process induced *in vivo* by hydrogel injection. (A) Dashed lines outline representative low magnification coronal sections of mouse spinal cord injected, three days before, with PCL loaded hydrogel (a−d, PCL) or PCL-Mino loaded hydrogel (e−h, PCL-Mino). CD11b staining in PCL-Mino treated mice shows a reduced proliferation/activation of microglia/macrophages around the site of injection compared to PCL mice. Microglia, CD11b (green); PCL-based NPs, RhB (red); CD11b staining pseudocolors image (d−h). Scale bar = 150 μm. (B,D) High magnification of spinal cord sections of a mouse treated with PCL-NPs (B;a) or with PCL-Mino NPs (B;b) representing, respectively, region 1 and 2 identified by dashed line in panel A. Insets represent three-dimensional details of microglia/macrophages around the lesion site in both PCL and PCL-Mino NPs. PCL-Mino NPs induce an evident morphological change toward a quiescent phenotype in CD11b positive microglia/macrophages that have uptaken PCL-Mino NPs compared to PCL treatment, and this deactivation is evident up to 15 DPI (D;a,b). Microglia, CD11b (green); PCL or PCL-Mino, RhB (red); cell nuclei, Hoechst (blue). Scale bar = 50 μm. (C,E) Evaluation of CD11b staining in a region of tissue up to 100 μm of distance from the site of injection at 3 DPI for PCL, PCL-Mino or free Mino loaded and injected with hydrogel (C;a,b) or 15 DPI for PCL and PCL-Mino loaded and injected with hydrogel (E;a,b). The analysis reveals a significant reduced microglia/macrophage proliferation/activation in mice treated with minocycline, mostly when it was loaded in NPs. Data are presented as mean ± SD. Statistical significance: (*)$p = 0.05$ ($n = 10$ for each group).

respectively to LPS (0.51 + 0.09 mean sphericity ± SD) and LPS+PCL (0.67 + 0.17 mean sphericity ± SD) stimulated cells (Figure 4A,C), but with a significantly lower efficacy compared to activated microglia treated with PCL-Mino (0.31 ± 0.13 mean sphericity ± SD). All groups showed an increased significant sphericity compared to CTR group (LPS, LPS+Mino, LPS+PCL, LPS+PCL+Mino $P = 0.001$ and LPS+PCL-Mino $P = 0.05$).

***In Vivo* Study of the Pharmacological Activity of Minocycline Delivered by PCL-Based NPs.** To determine the potential pharmacological activity of drugs delivered by the NP system previously described, we tested biodegradable PCL-based NPs loaded with minocycline *in vivo*. To do that, an injury induced by injected hydrogel was carried out in adult mice (as described in Experimental Section). We compared mice injected with unloaded PCL-based NPs (PCL), as control, free minocycline (Mino, 35 μg/mL) and minocycline encapsulated in PCL-based NPs (PCL-Mino, 35 μg/mL loaded) at two different times of evaluation, 3 and 15 DPI. *Ex vivo* analysis revealed a reduced proliferation of microglia/macrophages around the injured site in Mino mice at 3 DPI (Figure S4A, Supporting Information). Indeed, the quantification of CD11b staining around the lesion site, detected up to 100 μm from the center of the lesion, revealed that Mino treated mice had a significant

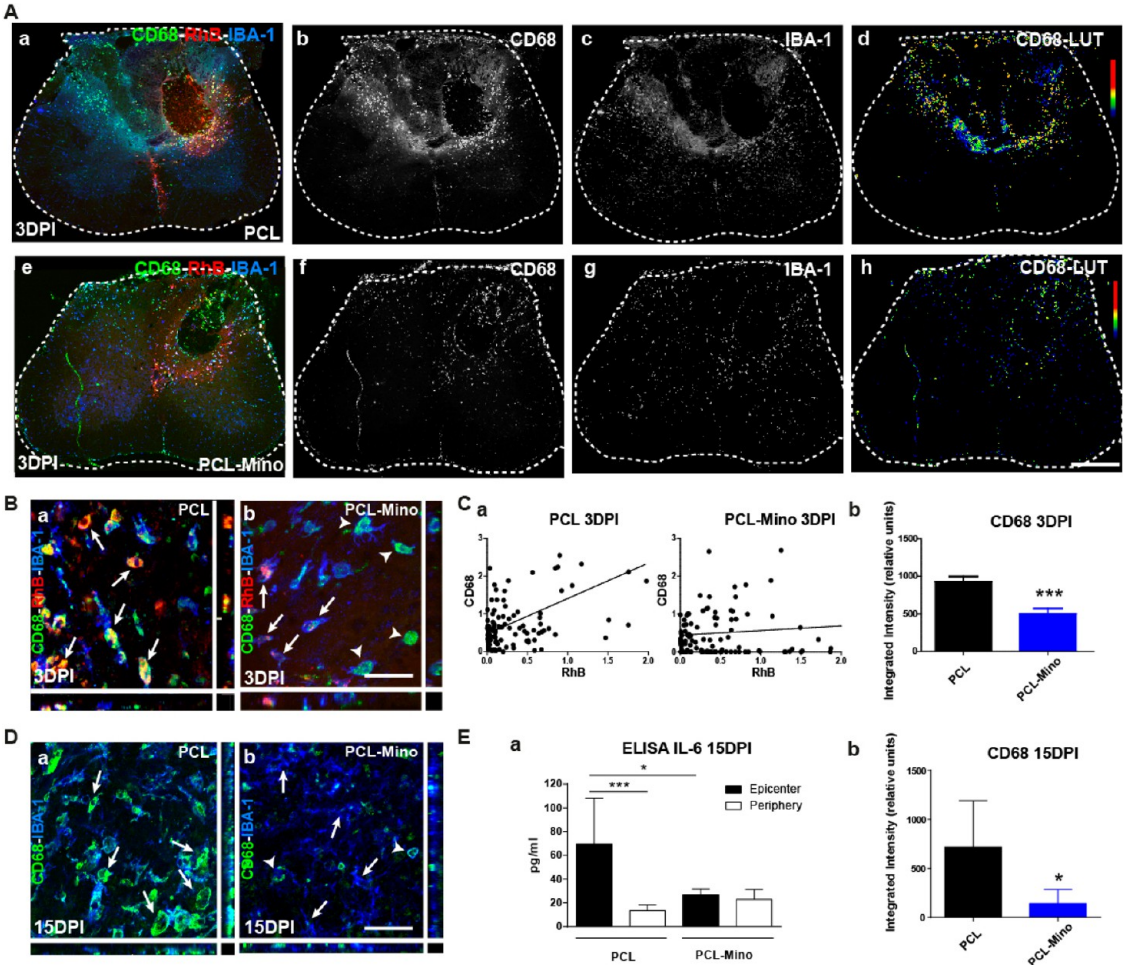

Figure 6. PCL-Mino NPs are able to reduce proinflammatory milieu after trauma *in vivo*. (A) Dashed lines outline representative low magnification of coronal sections of mice spinal cord injected with PCL-Mino NPs (e–h) or PCL NP loaded hydrogel (a–d). CD68 staining shows a lower signal in PCL-Mino treated mice (e,f,h) compared to control mice (a,b,d). Activated microglia/macrophage cells, CD68 (green); PCL or PCL-Mino, RhB (red); microglia, Iba-1 (blue). Scale bar = 150 μm. (B) High magnification of confocal image stack shows that microglia/macrophages with high level of PCL-Mino NPs internalized exhibits low level of CD68 staining after 3 DPI (b, arrows) compared to microglia/macrophages that did not uptake NPs (b, arrowheads) or microglia/macrophages that uptake PCL (a, arrows). (D) This effect is evident up to 15 DPI (a,b) where an increased number of round shape cells with high level of CD68 is found in PCL-based NPs treatment (a, arrows) compared to PCL-Mino treated mice (b, arrowheads). CD68 (green); PCL or PCL-Mino, RhB (red); microglia, Iba-1 (blue). Scale bar = 50 μm. (C) (a) Correlation analysis between CD68 staining and RhB signal, sampling single cells, at 3 DPI. A reduced correlation is evident for PLC-Mino treated mice compared to PCL. This is represented by different linear regression slope between them suggesting an effect of minocycline in reducing the CD68 level in microglia/macrophages after PCL-Mino uptake. (C,E) Quantitative analyses of CD68 staining respectively at 3 (C;b) or 15 DPI (E;b) show that a significant reduced staining of CD68 persists up to 15 DPI. (E;a) ELISA assay on spinal cord tissue homogenates shows a significant reduced level of cytokine IL-6 in the epicenter of the lesion in PCL-Mino compared to PCL treated mice at 15 DPI. Data are presented as mean ± SD. Statistical significance: (*)p = 0.05, (***)p = 0.001 (n = 10 for each group).

reduction (931 ± 283 mean integrated intensity ± SD) compared to control mice (PCL) (1630 ± 241 mean integrated intensity ± SD) (Figure 5C). However, the activated microglia/macrophages around the lesion in Mino treated mice still showed a round shape (Figure S4B, Supporting Information), suggesting a likely reduced proliferation of these cells without a clear morphological changing to quiescent phenotype. Analyzing PCL-Mino mice at 3 DPI, a significant reduction of CD11b staining was detected, suggesting a decreased proliferation and activation of microglial cells (767 ± 237 mean integrated intensity ± SD) (Figure 5A,C). Moreover, an evident morphological change toward a more quiescent phenotype (ameboid/resting shape) was found in RhB positive microglia/macrophages around the lesion (Figure 5B) compared to both PCL and Mino mice. To further confirm that NPs loaded with minocycline were able to reduce the activation state of microglia/macrophages from the phagocytic/ameboid to a more quiescent resting state, we investigated deeply the activation of the microglia/macrophage cells by studying the expression of CD68, a specific marker of activation and phagocytosis. A clear decrease of CD68 staining could be appreciated in PCL-Mino treated mice compared to mice injected with only PCL (Figure 6A). Moreover, many cells containing high

amount of PCL-Mino NPs showed low levels of CD68 compared to either cells that did not uptake NPs or cells that uptake unloaded NPs (Figure 6B). This was confirmed by the correlation analysis between CD68 staining and RhB signal for single cells, evaluated around the injury site, comparing PCL *versus* PCL-Mino mice (Figure 6C). This analysis highlighted a reduced level of CD68 staining in cells with a high RhB signal for PCL-Mino treated mice (0.08 Pearson coefficient) compared to PCL treated mice (0.50 Pearson coefficient-), which showed higher levels of CD68 in highly RhB positive cells. This was confirmed also by a quantitative evaluation of the overall CD68 staining comparing PCL-Mino to PCL mice around the injury site (Figure 6C).

To assess the duration of deactivation and/or limited proliferation of microglia/macrophages, the effect of the treatment here proposed was analyzed up to 15 DPI. At this time of analysis the fluorescent signal of PCL-based NPs is no longer detectable because of their degradation. However, a persistent reduced inflammatory state near the lesion site was found. In fact, a significant reduced staining of both CD11b and CD68 was revealed in PCL-Mino compared to PCL mice, the latter used as control (Figure S5A,B,D, Supporting Information). This was confirmed by the quantification of CD11b staining, comparing an equivalent region of tissue from the epicenter of the lesion in both PCL (1590 ± 243 mean integrated intensity $\pm$ SD) and PCL-Mino (1081 ± 174 mean integrated intensity $\pm$ SD) (Figure 5E). In addition, a significant persistent reduced activation of microglia/macrophages was demonstrated again by evaluation of CD68 staining for PCL-Mino (141 ± 54 mean integrated intensity $\pm$ SD) compared to PCL mice (721 ± 167 mean integrated intensity $\pm$ SD) (Figure 6Eb). Furthermore, an ELISA assay was carried out on spinal cord tissue homogenates at 15 DPI, which showed significantly reduced levels of the proinflammatory cytokine IL-6 in the epicenter of the lesion in PCL-Mino (26.6 ± 5.2 mean pg/mL $\pm$ SD) compared to PCL mice (69.6 ± 38.4 mean pg/mL $\pm$ SD) (Figure 6Ea). Conversely, at this time of analysis, IL-1β and TNFα cytokines did not show any significant difference between the epicenter and a more peripheral portion of tissue in rostral direction used as a control (data not shown), suggesting no relevant involvement of these cytokines during the progression of the degeneration in the traumatized site in this specific model.

DISCUSSION

Improved pharmacological approaches for limiting the progressive tissue degeneration and neuronal dysfunction after an acute spinal cord injury are needed. In this study we characterized a new pharmacological delivery tool able to release, with a cell-specific targeting, a well-known anti-inflammatory drug (minocycline) in the activated microglia/macrophages. Specifically, we characterized new polymeric PCL-based NPs, comparing them to PMMA and Qdot655. We demonstrated by *in vitro* and *in vivo* paradigms that polymer-based PCL-based NPs are the most promising for the treatment of this specific cell population because they are internalized mostly by the activated form of microglia/macrophages. In particular, we proved the following: (I) PCL-based NPs are captured exclusively by microglial cells in a short time (24−48 h). (II) Activated microglia (ameboid or phagocytic phenotype) are able to capture markedly these PCL-based NPs, whereas resting/unstimulated cells do not. (III) The cellular internalization of PCL-based NPs in activated microglia occurs *via* clathrin-dependent endocytotic pathway. (IV) PCL-based NPs show a complete biocompatibility when internalized in activated microglia/macrophages without inducing further proinflammatory stimuli or any toxicity. (V) After internalization into the cytosol PCL-based NPs do not affect the organelle ultrastructure in microglial cell. (VI) PCL-based NPs show a complete degradation by enzymatic lysosomal activity after 6 days in activated microglia/macrophages, whereas PMMA are not degraded and remain intact in MVB. (VII) The loading of PCL-based NPs with minocycline is able to reduce, *in vivo*, the activation and the proliferation of microglia/macrophages around the lesion site, turning them from a round shape phagocytic-like phenotype with high CD68 level to a more arborized resting phenotype with low CD68 staining. Round shape phenotype and increased high CD68 level were well characterized in different inflammatory milieu as markers for activated microglia/macrophages, and a reduced expression of them is considered predictive of the efficacy of anti-inflammatory treatments.[23,24] In addition, (VIII) the treatment here proposed limits, up to 15 days tested, the proinflammatory stimuli associated with microglia/macrophage activation,[9] as demonstrated by the reduced expression of the proinflammatory cytokine IL-6 in traumatized site.

Growing evidence showed that targeting and modulating microglial cells in the spinal cord injury could be a relevant therapeutic strategy.[25−27] In fact, several different pathophysiological events are associated with a prolonged microglia activation, such as a persistent inflammatory environment after the primary injury[3,8,28] and chronic neuropathic pain[29,30] that takes over in the progression of SCI. Recent findings have highlighted a dual role (detrimental or beneficial) related to different activated phenotypes of microglia/macrophages after the primary spinal cord injury:[6] proinflammatory cells (M1) or anti-inflammatory/reparative cells (M2). Detrimental effects have been associated with the M1 cells such as production of many proinflammatory mediators including cytokines (IL1β, IL-6, and TNFα), reactive oxygen species, and inducible nitric oxide synthase that contribute to the cascade of inflammatory events during the trauma.[6,31] M1 phenotype results already activated in an early stage after the primary injury (minutes) with a sustained

prolonged effect up to months.[6,8] On the other hand, M2 cells exert protective effects in terms of tissue repair and resolution of inflammation with a temporally limited effect (some days after injury).[32,33] It is well characterized that M1 subset is the most prominent activated phenotype during the progression of the trauma, suggesting that a lack in resolving the inflammation is one of the major drivers in worsening of the secondary injury of SCI.[8] This suggests that a long-term deactivation of microglial cells after the acute phase could be a promising strategy to counteract the detrimental contributing effect of a prolonged inflammatory response and chronic pain associated with spinal cord injury. So far different anti-inflammatory and painkiller treatments have been proposed, and only few of them were able to modulate the activation of the microglia and no one in a selective way.[5,25−27,34−36] Furthermore, most of these treatments antagonize only the acute inflammatory activation of microglial cells, whereas presence of activated microglia is still demonstrated up to months after the primary lesion of the spinal cord.[8,30] Among the drugs with a direct active effect on microglial cells, minocycline is one of the most promising.[25−27,35−37] In fact, in addition to the well-known antimicrobial activity, minocycline has been reported to have neuroprotective effects in various experimental models such as cerebral ischemia, amyotrophic lateral sclerosis, Parkinson's disease, Huntington disease, multiple sclerosis, traumatic brain injury, and SCI.[38] Recent studies have demonstrated anti-inflammatory, antiapoptotic, and antioxidant properties of minocycline in SCI.[27,35,36] Anti-inflammatory effects are mostly associated with the suppression of the proliferation and activation of the microglial cells and the subsequent release of cytokines such as IL-1β, TNFα, and IL-6, chemokines, and nitric oxide.[34,35,39] Furthermore, minocycline reduces TNF-α mRNA levels in SCI murine model, counteracting proinflammatory stimuli,[34] and reduces nitric oxide production after excitotoxic stimulus[26] in microglial cell cultures.

Thanks to their versatility in terms of size, potential surface, and hydrophilic or lipophilic characteristics, polymeric NPs lead relevant advantages in drug delivery by increasing the selectivity of drugs and by controlling their release during the time. In the past decade a large amount of different NP systems were studied and tested in SCI.[12] Among them only few studies[17,40] considered the possibility to target NPs to specific cell lines, and only Minami and co-workers showed high specificity to microglia using Qdot NPs.[17] So, compared to recent literature, we developed biocompatible NPs loaded with a well-known anti-inflammatory drug, minocycline, in order to demonstrate the selectivity and efficacy of PCL-based NPs as drug delivery tool, while several concerns arise on Q-Dots toxicity.[41] Furthermore, the selective and specific treatment of the microglia/macrophages here proposed shows different advantages compared to the conventional anti-inflammatory adminstration: (I) a drug delivery nanocarrier capable of directly targeting and modulating specific cells characterized by a proinflammatory phenotype during the subacute progression of the secondary injury in SCI; (II) a targeted delivery approach, as here proposed, is able to improve and maximize the therapeutic efficacy of anti-inflammatory compounds, by reducing the drug dose used in therapy and minimizing potential side effects; (III) a selective treatment in a such specific way represents a new potential tool able to modulate at different time during the secondary injury, with temporally defined NPs administration, the activation of the microglial cells, enhancing the beneficial role of the microglia during the progression of the disease; (IV) the polymeric PCL-based NPs here used exhibited high biocompatibility *in vitro* and *in vivo*.

CONCLUSIONS

In this study we have demonstrated the selective efficacy of minocycline loaded in biodegradable nanoparticles in reducing the inflammatory response mediated by microglia/macrophage activation, in a mouse model of SCI, but other diseases may also respond to such treatment. In fact many central nervous system diseases show microglia/macrophage inflammatory response, such as multiple sclerosis, Alzheimer's disease, Parkinson disease, amyotrophic lateral sclerosis, prion's disease, and epilepsy. Furthermore, this delivery strategy may be considered for other potential drugs such as molecules potentially able to induce a shift from M1 to M2 phenotype, leading to beneficial effects after the inflammatory response. Moreover, the approach here proposed, which is able to treat selectively inflammatory cells using biodegradable nanoparticles with a well-known drug (minocycline) used in different human pathologies (antibiotic activity), opens a new translational avenue to the inflammatory and pain treatment in SCI patients.

EXPERIMENTAL SECTION

Preparation of Nanoparticles

Materials. Rhodamine B (RhB, Sb sensitivity <0.1 $\mu g \cdot mL^{-1}$, Carlo Erba reagents), 2-hydroxyethyl methacrylate (HEMA; 97% purity, ABCR), dicyclohexylcarbodiimide (DCC; 99% purity, Sigma-Aldrich), 4-(dimethylamino)-pyridine (DMAP; >99% purity, Sigma-Aldrich), acetonitrile (ACN, ≥99.9% purity, Sigma-Aldrich), ε-caprolactone (CL, 99%, Sigma-Aldrich), 2-ethylhexanoic acid tin(II) salt ($Sn(Oct)_2$, ~95%, Sigma-Aldrich), potassium persulfate (KPS; >99% purity, ACS reagent), poly(ethylene glycol) methyl ether methacrylate (HEMA-PEG_{19}, molecular weight: ca. 950 Da) (Sigma-Aldrich), and polyoxyethylenesorbitan monooleate (Tween80; Sigma-Aldrich) were used for nanoparticles (NPs) synthesis as received. For size exclusion chromatography (SEC) analysis tetrahydrofuran (THF, ≥ 99.7%, Sigma) was used as

eluent, for HPLC analyses, acetonitrile, ammonium acetate, and methanol were used, all purchased from Sigma-Aldrich. ^{1}H NMR experiments were performed in $CDCl_3$ (sigma-Aldrich).

Synthesis and Characterization of RhB-Based Macromonomer. RhB was used as fluorescent dye to detect NPs. In order to avoid the dye desorption from the NPs itself, RhB was covalently bonded to HEMA, an FDA approved molecule commonly used for contact lenses production. It is a polymerizable compound, obtained through an esterification reaction and then copolymerized with other monomers obtaining NPs with RhB covalently linked to the polymer matrix. DCC was used as an esterification agent to covalently bond RhB to the HEMA molecule adopting DMAP as a catalyst. The reaction was performed in acetonitrile, and all the details on the synthesis and characterization are reported in the Supporting Information. Briefly, RhB and HEMA were dissolved in acetonitrile and loaded together in a beaker, while DCC and DMAP, both dissolved in acetonitrile, were added dropwise. The reaction was run for 24 h at 40 °C under magnetic stirring. After that, reaction media were quenched in an ice bath, and the dicyclohexylurea (DCU) coming from the DCC hydration was removed by filtration. Dried macromonomer (HEMA-RhB) was obtained from acetonitrile removal by solvent evaporation under a vacuum. The raw product was chromatographically purified through HPLC, as described in the Supporting Information. A detailed characterization of the macromonomers is also reported in the Supporting Information. The absence of free RhB in the aqueous solution, together with the behavior in *in vitro* conditions of the Fluorescent NPs, have already been shown.[42,43]

Synthesis and Characterization of HEMA-CL_3 and HEMA-PEG_{19} Macromonomers. The macromonomer used for the NPs synthesis was synthesized through a ring-opening polymerization reaction (ROP) using a procedure reported in literature.[19] Reaction was carried out in bulk conditions, without using any solvent. Ten grams of CL were heated up in a stirred flask at 130 ± 1 °C with the temperature controlled by an external oil bath. A mixture of $Sn(Oct)_2$ and HEMA at a given molar ratio (1/200) was prepared and left under continuous magnetic stirring at room temperature until the complete dissolution of $Sn(Oct)_2$. Then, HEMA solution (composed of 3.8 g of HEMA and 29 mg of $Sn(Oct)_2$) was then added to CL (CL/HEMA molar ratio equal to 3) to initiate the reaction, which was carried out for 2 h. The reaction product (HEMA-CL_3 macromonomer) was refrigerated at 4 °C waiting for further use.

Macromonomer molecular weight (MW) and thus the average chain length *n* (the average number of CL unit added to HEMA molecule, theoretically equal to 3 in this work) characterization has been carried out combining size exclusion chromatography SEC with ^{1}H NMR analysis. In addition, the average chain length (here theoretically equal to 19.2) of commercially available HEMA-PEG_{19} macromonomer, used in the further emulsion polymerization reaction, was confirmed by ^{1}H NMR measurement.

Details of the SEC and ^{1}H NMR apparatus, as well as the detailed macromonomers characterization, are collected in the Supporting Information.

Poly(HEMA-g-CL_3)-Based NPs and Poly(Methyl Methacrylate)-Based NPs Synthesis and Characterization. PCL and PMMA-based NPs were synthesized through free radical emulsion polymerization performed in a monomer starved semibatch emulsion polymerization (MSSEP)[19] by using KPS as initiators and Tween80 as surfactant. Reaction was carried out using a 100 mL three necked glass flask equipped with a reflux condenser. Temperature was controlled with an external oil bath set to 80 ± 1 °C. The reactor was kept inert through vacuum-nitrogen cycles.

The MSSEP procedure used to produce PEGylated PCL or PMMA-based NPs consists in the loading of the hydrophilic macromonomer (HEMA-PEG_{19} in this case) in the reactor as in a normal batch polymerization, while the more hydrophobic monomer (HEMA-CL_3 or MMA) is injected in a semibatch process. More detailed Tween80 and HEMA-PEG_{19} were added to 45 mL of deionized water. Then, the solution of the two monomers (HEMA-CL_3 or MMA and HEMA-RhB) was injected into the system with a flow rate of 3 mL/h using a syringe pump (Model NE-300, New Era Pump System, Farmingdale, US) after the initiator injection (dissolved in 2.5 mL of water) in the purged solution. The system was maintained under magnetic stirring at 350 rpm, reaction was run for three hours, and the final monomer conversions were measured through ^{1}H NMR and calculated as higher than 99.5%. After the NP synthesis the pH of the solution was adjusted to 7 using NaOH 0.1 M. The total amount of involved monomers was 2.5 g in order to ensure a final solid content of 5% w/w. In particular, PEGylated NPs were obtained using the following recipes:

PEGylated PCL-based NPs: 10% Tween80/Monomer ratio, 0.5 g HEMA-PEG_{19}, 2 g of HEMA-CL_3, 25 mg of HEMA-RhB, 0.04 g of KPS.

PEGylated PMMA-based NPs: 5% Tween80/Monomer ratio, 0.5 g HEMA-PEG_{19}, 2g of MMA, 25 mg of HEMA-RhB, 0.04 g of KPS.

Non-PEGylated PCL-based NPs were obtained through a MSSEP process as described above, without the use of HEMA-PEG_{19}; in particular, the following recipe was adopted:

PCL-based NPs: 20% Tween80/Monomer ratio, 2.5 g of HEMA-CL_3, 25 mg of HEMA-RhB, 0.04 g of KPS.

NP Characterization. Data about size and particle size distribution (PSD) of NP suspensions have been determined through dynamic light scattering (DLS) measurements (Malvern, Zetanano ZS). In addition, the stability of these NPs has been verified, maintaining the NPs for 48 h at 37 °C in the same medium used for the cellular growth. Detailed NP distribution after synthesis and incubation with cell medium from the DLS are reported in the Supporting Information. ^{1}H NMR was performed using a 500 MHz Ultrashield NMR spectrometer (Bruker, Switzerland) by dissolving the sample in DMSO-d_6 (Sigma).

Animals and Their Care. Procedures involving animals and their care were conducted in conformity with the institutional guidelines that comply with national (D.L. n. 116, G.U., suppl. 40, Feb. 18, 1992, Circolare No. 8, G.U., July 14, 1994) and international laws and policies (EEC Council Directive 86/609, OJL 358, 1, December 12, 1987; Guide for the Care and Use of Laboratory Animals, U.S. National Research Council, 1996).

Primary Cell Cultures. Primary cultures of microglia or neuron/glia cocultures were obtained from the spinal cord of 13-days-old C57BL/6J (Charles River Laboratories International, Inc.) and B6.129P-Cx3cr1tm1Litt/J (The Jackson Laboratory) mouse embryos, as previously described.[44] Briefly, spinal cords were dissected, exposed to DNase and trypsin (Sigma-Aldrich, Milan, Italy), and centrifuged through a BSA cushion. Cells obtained at this step were a mixed neuron/glia population and underwent centrifugation through a 6% iodixanol (OptiPrep, Sigma-Aldrich) cushion to separate large neurons from glial cells. The glial feeder layer was prepared by plating the glial fraction at a density of 25 000 cells/cm^2 into 12-well plates or into flasks, both previously precoated with poly-L-lysine (Sigma-Aldrich). Purified microglia were obtained from flasks containing confluent mixed glial cultures after overnight shaking at 275 rpm in incubators. The supernatants (containing microglia) were collected and seeded at a density of 20 000 cells/cm^2. Astrocyte cultures were obtained by treating the glial cultures, from which microglia had been previously harvested, with 60 mM L-leucine methyl ester (Sigma-Aldrich) for 90 min. To establish neuron/glia cocultures, the neuron-enriched fraction (obtained from the iodixanol-based separation) was seeded at a density of 10 000 cells/cm^2 onto a mature astrocyte layer, and microglia were added (10% of the astrocyte number) on the third day *in vitro*.

Culture Treatments. Microglia activation was induced by exposing purified microglia cultures or neuron/glia cocultures to 1 μg/mL of LPS (from *Escherichia coli* 0111:B4; Sigma-Aldrich) for 18 h, as previously reported by De Paola *et al.*[44] Cultures maintained with normal medium served as the control condition. Different NP species (PMMA-based, PCL-based and Qdots655) were then added to untreated or LPS-stimulated cultures. For the chlorpromazine hydrochloride (CPZ; Sigma-Aldrich) treatments, different solutions of CPZ (final concentrations: 30, 40, or 50 μM) were added to the culture medium 2 h before NPs exposure. CPZ did not show neurotoxicity up to 40 μM.

Cell Viability Assay. The CellTiter Aqueous Non-Radioactive Cell Proliferation Assay (MTS; Promega, Italy) and propidium

iodide (1 μg/mL, AbD Serotec, Italy) were used according to the manufacturer's instruction to determine cell viability in NPs treated microglia cultures.

Immunocytochemistry. Cells were fixed with 4% paraformaldehyde and permeabilized by 0.2% Triton X-100 (Sigma-Aldrich). Staining was carried out by overnight incubation with the primary antibodies, followed by incubation with an appropriate fluorescent secondary antibody. Cell nuclei were labeled with Hoechst 33258 (Invitrogen) by incubation with a 250 ng/mL solution. Double or triple staining was carried out by overnight incubation of the cultures separately with each primary antibody. In each experiment, some wells were processed without the primary antibody to verify the specificity of the staining. The following primary antibodies were used: antineurofilament 200 (rabbit, 1:500; Sigma-Aldrich); anti-GFAP (rabbit, 1:500; Millipore); anti-CD11b (rat, 1:1000; eBioscience Inc.); anti-CD68 (rat, 1:500; AbD Serotec); anti-Iba 1 (rabbit, 1:500; Wako Chemicals Gmbh). Appropriate fluorescent secondary antibodies (Dylight; Rockland Immunochemicals, Inc.) conjugated to different fluorochromes were used at 1:1000 dilution. For lysosomal activity analyses a lysosensor dye, which becomes more fluorescent in acidic environments (1:20.000 dilution, Life Technologies), was used. For the membrane staining, we used the wheat germ agglutinin (WGA) Alexa fluor 350 conjugated (5 μg/mL, Life Technologies).

Quantitative Enzyme-Linked Immunosorbent Assays (ELISA). TNFα, IL-6, and IL-1β concentrations for both cell culture supernatant and homogenate of spinal cord tissues were quantified by solid-phase sandwich ELISA (eBioscience, Inc.). Samples from each experiment were tested in triplicate, according to the manufacturer's instructions.

Transmission Electron Microscopy. A 5 μL drop of purified PCL and PMMA in PBS was placed to dry at room temperature on a 100 mesh Formvar/carbon coated copper grid (EMS, Hatfield, PA, USA) and observed with an Energy Filter Transmission Electron Microscope (EFTEM, Zeiss Libra 120) equipped with YAG scintillator slow scan CCD camera. Microglia cells were plated on glass coverslips and exposed to NPs for 1 and 6 days (PMMA) and 2 and 6 days (PCL). After incubation, medium was discarded and cells were prefixed for 10 min at rt with 4% paraformaldehyde and 1% glutaraldehyde in Hepes 0.2 M (pH 7.4) and fixed at 4 °C in 1% glutaraldehyde in Hepes 0.2 M, pH 7.4 until use. After 30 min incubation with osmium 1% in 0.12 M phosphate buffer pH 7.4 on ice, cells were incubated 5 min at rt with a saturated solution of thiocarbohydrazide followed by 1.5% ferrocianide and 1% osmium for 30 min. Microglial cells, still attached on the coverslip, were then counterstained with 0.5% uranyl acetate overnight at 4 °C and, after dehydration in graded series of ethanol, were embedded in Epoxy medium (Epon 812 Fluka, Sigma-Aldrich). Thereafter, coverslip was removed from the well of multiwell plate and, to allow the transfer of cells from coverslip to resin block, was placed bottom up on disposable flat embedding mold (Electron Microscopy Sciences) prefilled with Epoxy resin and polymerized at 60 °C for 72 h. After removing the glass coverslip using 40% fluorhydric acid, resin block with neurons on the top was trimmed to obtain a small pyramid suitable for ultrathin (55−60 nm thick) sectioning with a Leica EM UC6 ultramicrotome. Sections were then collected on 100 mesh Formvar carbon-coated grids and examined with an EFTEM equipped with a YAG scintillator slow scan CCD camera (Zeiss).

Loading of Minocycline in PCL-Based NPs. Since NP synthesis has been carried using an emulsion polymerization process, the drug loading step could not take place during NP formation because of the presence of both high temperature and radicals; therefore, a postsynthesis process has been set up. First NPs latex concentration was increased up to 5% w/w under a vacuum; the absence of NPs coalescence during this step was confirmed by DLS measurements. Minocycline-base was preliminarily obtained from minocycline hydrochloride (Sigma-Aldrich, CAS 13614-98-7) in order to increase its hydrophobicity and consequently the loading efficiency. Minocycline hydrochloride was converted into its free base before being loaded within NPs to increase its hydrophobicity and consequently the percentage of loading. Briefly, minocycline hydrochloride (10 mg) was dissolved in a saturated solution of sodium bicarbonate (2 mL). Then the aqueous solution was extracted four times with dichloromethane (4 × 2 mL). The organic phase was separated and then dried over sodium sulfate, filtered, and concentrated under reduced pressure. The resulting powder (8 mg, 80% yield) was then dissolved in DMSO at a concentration of 2 mg/mL. The drug loading procedure is facilitated since the NPs are naturally constituted of a hydrophobic core and a hydrophilic shell constituted of PEG chains.[45] The drug was entrapped in the partially swollen preformed NPs in the following way: a PTFE cylinder of 1 cm of diameter and 1 cm of length with an axial perforation of 1 mm diameter and a radial one of 500 μm was used as a mixing device for the drug loading procedure (see Supporting Information for a detailed representation of the apparatus, Figure S9, Supporting Information). The NP latex (300 mg in 6 mL of deionized water, concentration of 50 mg_{NPs}/mL_{water}) and the dissolved drug (2 mg of minocycline in 1 mL of DMSO) were loaded in syringe pumps and injected radially in the device at a flow rate of 30 and 5 mL/min, respectively. Four-hour dialysis was employed to remove free minocycline, as preliminarily checked (Figure S4D, Supporting Information). The amount of minocycline present in PLC-based NPs at the end of the dialysis period was determined by HPLC−MS/MS. For that, aliquots were added with IS and 10 volumes of chloroform:isopropanol (1:1), shaken for 5 min and centrifuged at 13 000 rpm for 10 min. Supernatants were dried under a gentle nitrogen stream at room temperature, and samples were finally reconstituted in acetonitrile (ACN, Sigma-Aldrich) containing 0.1% formic acid to be injected in the HPLC−MS/MS system maintained at 6 °C. Stock solutions of minocycline hydrochloride (Sigma-Aldrich) and demeclocycline hydrochloride (Sigma-Aldrich), used as internal standard (IS), were prepared in methanol and kept at −20 °C until use. All chemicals (formic acid, isopropanol, and chloroform, Carlo Erba) used were of analytical or HPLC−MS grade. The HPLC system consisted of an Alliance separation module 2695 coupled with a Micromass Quattro Micro triple quadrupole mass spectrometer (Waters) controlled by Mass Lynx software 4.1. The mass spectrometer operated in positive ion and multiple reaction monitoring (MRM) mode, measuring the fragmentation products of molecular ions of substances. The instrument is equipped with an electrospray ionization interface and uses argon as collision gas. Source and desolvation temperatures were set at 100 and 300 °C, respectively. Samples were analyzed with the ion spray needle operating at 4.8 kV, the cone voltage at 25 V, and the collision energy at 15 eV. The principal ion transition 458.1 > 441.2 was selected for minocycline quantification, while the transition 465.0 > 448.3 was selected for IS. Chromatographic separation was achieved on a Waters XTerra MS C18 column (100 × 2.1 mm, 3.5 μm) coupled with an XTerra C18 cartridge, held at 30 °C. The mobile phases consisted of water (MP-A) and ACN (MP-B), both containing 0.1% formic acid. The HPLC system was set up to operate at a flow rate of 0.2 mL/min at a the following linear gradient: from 2 to 98% MP-B in 15 min, at 98% MP-B for 3 min, from 98 to 2% MP-B in 1 min (total run time 30 min). The retention times were 9.9 min for minocycline and 11.3 min for IS.

Hydrogel Synthesis. Hydrogels (AC) were prepared by blocking polymerization in PBS at about 80 °C, where polymeric solution (carbomer 974P 0.5 wt %, agarose 0.5 wt %) was achieved by mixing polymer powders into the selected solvent, adding a mixture of cross-linking agents primarily made of propylene glycol (30 wt %) and glycerol (1.2 wt %) (along with NaOH 1 N 3 wt % for pH neutralization). Reaction pH was indeed kept neutral. Gelation start was achieved by means of microwave (EM) stimulation. Effective gelation and reticulation were achieved by microwave heating for 1 min per 10 mL of polymeric solution.[22]

Surgery. Before surgery the animals received an antibiotic and analgesic treatment, respectively with a subcutaneous injection of ampicillin (50 mg/kg) and buprenorphine (0.15 mg/kg). Entire surgical procedure was carried out in deep anesthesia by ketamine hydrochloride (IMALGENE, 100 mg/kg) and medetomidine hydrochloride (DOMITOR, 1 mg/kg) intraperitoneally. Animals were placed on a Cunningham Spinal Cord Adaptor

(Stoelting, Dublin, Ireland) mounted on a stereotaxic frame, and laminectomy of T12 vertebra was done to uncover the lumbar spinal cord. Using a glass capillary (40 ± 2 μm diameter) the hydrogel AC solution (0.5 μL/site) was injected in the spinal cord with a flow rate of 0.2 μL/min. Stereotaxic coordinates were referred to the midline of the dorsal horn of the spinal cord. The needle was positioned at +0.5 mm aside from the midline, and then it was deepened into the parenchyma to 0.7 mm below the pia mater.

The injector was left in place for 1 min and then retracted for 0.2 mm before starting the delivery. After gel injection, the needle was left in place for an additional 3 min and then gently withdrawn.

Spinal Cord Transcardial Perfusion. At selected time, mice were deeply anesthetized with ketamine hydrochloride (IMALGENE, 100 mg/kg) and medetomidine hydrochloride (DOMITOR, 1 mg/kg) and transcardially perfused with 40 mL of PBS, 0.1 mol/liter, pH 7.4, followed by 50 mL of sodium phosphate buffered 4% paraformaldehyde solution. Spinal cords were rapidly removed, postfixed for 2 h, transferred to 30% sucrose in PBS at 4 °C overnight for cryoprotection and stored at 4 °C until use.

ELISA analysis was carried out on mice tissues transcardially perfused with 40 mL of PBS, 0.1 mol/liter, pH 7.4. Spinal cords were rapidly removed, frozen on dry ice and then homogenized in 4 volumes of 5X assay diluent provided in the ELISA kit. For each animal the spinal cord area around the site of injection (±5 mm from the epicenter) and a peripheral part of cord as internal control were removed and frozen.

Preparation of Spinal Cord Sections. Spinal cord area around the site of injection (±5 mm from the epicenter) was embedded in OCT compound and frozen by immersion in *N*-pentane at −45 °C for 3 min and then stored at −80 °C until use. Frozen tissues were sectioned in 30 μm coronal sections on a cryostat at −20 °C. Serial sections were collected in PBS with sodium azide (0.02%) and stored at 4 °C until use.

Immunofluorescence. Imunofluorescence was performed on 30 μm coronal spinal cord sections. Sections were incubated with different primary antibodies dissolved in PBS, 1% normal goat serum and 0.1% Triton X-100 and incubated overnight at 4 °C under constant shaking. Astrocytes were stained with a mouse monoclonal antibody directed to GFAP (Glial Fibrillary Acidic Protein;, 1:2500 dilution, Millipore). Microglia were revealed using a rat monoclonal antibody anti-CD11b (specific for the complement C3 receptor of macrophages/monocytes/microglia, 1 μg/mL, produced by the Laboratory of Immunology and Inflammation, IRCCS Clinical Institute "Humanitas", Italy) or a polyclonal antibody directed to Iba-1 (ionized calcium binding adapter molecule, 1:1.1000 dilution, Wako). To detect specifically activated and phagocytic microglia, we used a rat monoclonal antibody directed to CD68 (1:200 dilution, AbD serotec). To label neuronal cells, spinal cord sections were stained with NeuroTrace Fluorescent Nissl Stain (1:500 dilution, Life Technologies, fluorescence excitation/emission maxima 640−660 nm).

Sections were then processed with specific secondary antibodies conjugated to Alexa Fluor (1:500 dilution, Life Technologies). Finally, spinal cord sections were mounted on slides and coverslipped with a 50% glycerol solution in PBS to proceed with acquisition by confocal microscope.

Immunofluorescence Quantification. Fluorescent signal was quantified thanks to the free software Fiji (http://fiji.sc/Downloads). Single cells (about 200) were surrounded with the "free hand" selection, and the integrated density of the signal was taken into consideration, as a representative value of both signal intensity and area of the staining.

For the evaluation of the cell sphericity, considered an index of microglial cells activation, single cells (about 200) were surrounded, and the "shape descriptors" were calculated through the software Fiji. For each cell, the software gives a value of sphericity ranging from 0 to 1, the last representing a perfect sphere. For the quantification of the CD11b staining in the area around the lesion, a specific plugin of Fiji was used (radial profile plot, http://rsbweb.nih.gov/ij/plugins/radial-profile.html). This plugin produces concentric circles around the epicenter of the lesion and gives a graph of the integrated density of the pixel values around each circle. We evaluated up to 100 μm of distance outside the epicenter of the lesion. For the correlation between CD68 expression and cellular uptake of NPs (about 200 cells evaluated), the integrated density of each staining was plotted on a graph, and Person's correlation analysis was taken into account.

Microscopy. Fluorescent NPs signal was acquired by using a 40× objective magnification, BX81 microscope and Fluoview II camera (Olympus). Colocalization studies were carried out by confocal microscope by using 40× objective magnification, BX81 microscope, FV1000 confocal (Olympus). Time lapse analysis was performed by using 60× objective magnification, Cell R station (Olympus), ORCA camera (Hamamatsu).

Statistical Analysis. Data were processed using Prism 6 software (Graphpad). Values are reported as mean ± SEM or mean ± SD. Mann−Whitney rank sum test was performed to test the significance among groups for *in vitro* NP uptake assessment, *in vivo* evaluation of CD11B staining at 15DPI, *in vivo* evaluation of CD68 staining at both 3 and 15 DPI. Kruskal−Wallis and *post hoc* analysis (Dunn's test) was performed to test the significance among groups for *in vitro* NP uptake assessment after CPZ treatment, *in vitro* ELISA assay, *in vitro* evaluation of cell sphericity, *in vivo* evaluation of CD11b staining at 3 DPI, whereas a two-way ANOVA and *post hoc* analysis (Tukey's test) was performed to test the significance among groups for *in vivo* ELISA assay. $P < 0.05$ was considered as statistically significant for all analysis.

Conflict of Interest: The authors declare no competing financial interest.

Acknowledgment. Authors' research is supported by Fondazione Cariplo, Grant No. 2010/0639. Authors would like to thank Dr. Alessandro Sacchetti for fruitful discussion.

Supporting Information Available: Supporting data including QDot655 cell uptake, TEM, MTS, ELISA, minocycline loading and macromonomer synthesis and characterization. This material is available free of charge *via* the Internet at http://pubs.acs.org.

REFERENCES AND NOTES

1. Illis, L. S. Central Nervous System Regeneration Does Not Occur. *Spinal Cord* **2012**, *50*, 259–263.
2. Borgens, R. B.; Liu-Snyder, P. Understanding Secondary Injury. *Q. Rev. Biol.* **2012**, *87*, 89–127.
3. David, S.; Kroner, A. Repertoire of Microglial and Macrophage Responses after Spinal Cord Injury. *Nat. Rev. Neurosci.* **2011**, *12*, 388–399.
4. Hulsebosch, C. E.; Hains, B. C.; Crown, E. D.; Carlton, S. M. Mechanisms of Chronic Central Neuropathic Pain after Spinal Cord Injury. *Brain Res. Rev.* **2009**, *60*, 202–213.
5. Loane, D. J.; Byrnes, K. R. Role of Microglia in Neurotrauma. *Neurotherapeutics* **2010**, *7*, 366–377.
6. Kigerl, K. A.; Gensel, J. C.; Ankeny, D. P.; Alexander, J. K.; Donnelly, D. J.; Popovich, P. G. Identification of Two Distinct Macrophage Subsets with Divergent Effects Causing Either Neurotoxicity or Regeneration in the Injured Mouse Spinal Cord. *J. Neurosci.* **2009**, *29*, 13435–13444.
7. Shechter, R.; Miller, O.; Yovel, G.; Rosenzweig, N.; London, A.; Ruckh, J.; Kim, K. W.; Klein, E.; Kalchenko, V.; Bendel, P.; *et al.* Recruitment of Beneficial M2 Macrophages to Injured Spinal Cord Is Orchestrated by Remote Brain Choroid Plexus. *Immunity* **2013**, *38*, 555–569.
8. Beck, K. D.; Nguyen, H. X.; Galvan, M. D.; Salazar, D. L.; Woodruff, T. M.; Anderson, A. J. Quantitative Analysis of Cellular Inflammation after Traumatic Spinal Cord Injury: Evidence for a Multiphasic Inflammatory Response in the Acute to Chronic Environment. *Brain* **2010**, *133*, 433–447.
9. Yang, L.; Jones, N. R.; Blumbergs, P. C.; Van Den Heuvel, C.; Moore, E. J.; Manavis, J.; Sarvestani, G. T.; Ghabriel, M. N. Severity-Dependent Expression of Pro-Inflammatory Cytokines in Traumatic Spinal Cord Injury in the Rat. *J. Clin. Neurosci.* **2005**, *12*, 276–284.
10. Perale, G.; Rossi, F.; Sundstrom, E.; Bacchiega, S.; Masi, M.; Forloni, G.; Veglianese, P. Hydrogels in Spinal Cord Injury Repair Strategies. *ACS Chem. Neurosci.* **2011**, *2*, 336–345.

11. Perale, G.; Rossi, F.; Santoro, M.; Peviani, M.; Papa, S.; Llupi, D.; Torriani, P.; Micotti, E.; Previdi, S.; Cervo, L.; *et al.* Multiple Drug Delivery Hydrogel System for Spinal Cord Injury Repair Strategies. *J. Controlled Release* **2012**, *159*, 271–280.
12. Rossi, F.; Perale, G.; Papa, S.; Forloni, G.; Veglianese, P. Current Options for Drug Delivery to the Spinal Cord. *Expert Opin. Drug Delivery* **2013**, *10*, 385–396.
13. Lee, H.; McKeon, R. J.; Bellamkonda, R. V. Sustained Delivery of Thermostabilized chABC Enhances Axonal Sprouting and Functional Recovery after Spinal Cord Injury. *Proc. Natl. Acad. Sci. U. S. A.* **2010**, *107*, 3340–3345.
14. Mout, R.; Moyano, D. F.; Rana, S.; Rotello, V. M. Surface Functionalization of Nanoparticles for Nanomedicine. *Chem. Soc. Rev.* **2012**, *41*, 2539–2544.
15. Shi, Y. Z.; Kim, S.; Huff, T. B.; Borgens, R. B.; Park, K.; Shi, R. Y.; Cheng, J. X. Effective Repair of Traumatically Injured Spinal Cord by Nanoscale Block Copolymer Micelles. *Nat. Nanotechnol.* **2010**, *5*, 80–87.
16. Jain, N. K.; Mishra, V.; Mehra, N. K. Targeted Drug Delivery to Macrophages. *Expert Opin. Drug Delivery* **2013**, *10*, 353–367.
17. Minami, S. S.; Sun, B.; Popat, K.; Kauppinen, T.; Pleiss, M.; Zhou, Y.; Ward, M. E.; Floreancig, P.; Mucke, L.; Desai, T.; *et al.* Selective Targeting of Microglia by Quantum Dots. *J. Neuroinflammation* **2012**, *9*, 22.
18. Sharma, G.; Valenta, D. T.; Altman, Y.; Harvey, S.; Xie, H.; Mitragotri, S.; Smith, J. W. Polymer Particle Shape Independently Influences Binding and Internalization by Macrophages. *J. Controlled Release* **2010**, *147*, 408–412.
19. Ferrari, R.; Yu, Y. C.; Morbidelli, M.; Hutchinson, R. A.; Moscatelli, D. epsilon-Caprolactone-Based Macromonomers Suitable for Biodegradable Nanoparticles Synthesis through Free Radical Polymerization. *Macromolecules* **2011**, *44*, 9205–9212.
20. Ferrari, R.; Colombo, C.; Dossi, M.; Moscatelli, D. Tunable PLGA-Based Nanoparticles Synthesized Through Free-Radical Polymerization. *Macromol. Mater. Eng.* **2013**, *298*, 730–739.
21. Yu, Y.; Ferrari, R.; Lattuada, M.; Storti, G.; Morbidelli, M.; Moscatelli, D. PLA-Based Nanoparticles with Tunable Hydrophobicity and Degradation Kinetics. *J. Polym. Sci., Part A: Polym. Chem.* **2012**, *50*, 5191–5200.
22. Perale, G.; Veglianese, P.; Rossi, F.; Peviani, M.; Santoro, M.; Llupi, D.; Micotti, E.; Forloni, G.; Masi, M. *In Situ* Agar-Carbomer Hydrogel Polycondensation: A Chemical Approach to Regenerative Medicine. *Mater. Lett.* **2011**, *65*, 1688–1692.
23. Fleming, J. C.; Norenberg, M. D.; Ramsay, D. A.; Dekaban, G. A.; Marcillo, A. E.; Saenz, A. D.; Pasquale-Styles, M.; Dietrich, W. D.; Weaver, L. C. The Cellular Inflammatory Response in Human Spinal Cords after Injury. *Brain* **2006**, *129*, 3249–3269.
24. Arnold, S. A.; Hagg, T. Anti-Inflammatory Treatments During the Chronic Phase of Spinal Cord Injury Improve Locomotor Function in Adult Mice. *J. Neurotrauma* **2011**, *28*, 1995–2002.
25. Festoff, B. W.; Ameenuddin, S.; Arnold, P. M.; Wong, A.; Santacruz, K. S.; Citron, B. A. Minocycline Neuroprotects, Reduces Microgliosis, and Inhibits Caspase Protease Expression Early after Spinal Cord Injury. *J. Neurochem.* **2006**, *97*, 1314–1326.
26. Tikka, T.; Fiebich, B. L.; Goldsteins, G.; Keinanen, R.; Koistinaho, J. Minocycline, a Tetracycline Derivative, is Neuroprotective against Excitotoxicity by Inhibiting Activation and Proliferation of Microglia. *J. Neurosci.* **2001**, *21*, 2580–2588.
27. Yune, T. Y.; Lee, J. Y.; Jung, G. Y.; Kim, S. J.; Jiang, M. H.; Kim, Y. C.; Oh, Y. J.; Markelonis, G. J.; Oh, T. H. Minocycline Alleviates Death of Oligodendrocytes by Inhibiting Pro-Nerve Growth Factor Production in Microglia after Spinal Cord Injury. *J. Neurosci.* **2007**, *27*, 7751–7761.
28. Donnelly, D. J.; Popovich, P. G. Inflammation and its Role in Neuroprotection, Axonal Regeneration and Functional Recovery after Spinal Cord Injury. *Exp. Neurol.* **2008**, *209*, 378–388.
29. Tsuda, M.; Beggs, S.; Salter, M. W.; Inoue, K. Microglia and Intractable Chronic Pain. *Glia* **2013**, *61*, 55–61.
30. Gwak, Y. S.; Kang, J.; Unabia, G. C.; Hulsebosch, C. E. Spatial and Temporal Activation of Spinal Glial Cells: Role of Gliopathy in Central Neuropathic Pain Following Spinal Cord Injury in Rats. *Exp. Neurol.* **2012**, *234*, 362–372.
31. Shechter, R.; Schwartz, M. Harnessing Monocyte-Derived Macrophages to Control Central Nervous System Pathologies: No Longer 'If' But 'How'. *J. Pathol.* **2013**, *229*, 332–346.
32. Neumann, H.; Kotter, M. R.; Franklin, R. J. Debris Clearance by Microglia: an Essential Link between Degeneration and Regeneration. *Brain* **2009**, *132*, 288–295.
33. Cardona, A. E.; Pioro, E. P.; Sasse, M. E.; Kostenko, V.; Cardona, S. M.; Dijkstra, I. M.; Huang, D.; Kidd, G.; Dombrowski, S.; Dutta, R.; *et al.* Control of Microglial Neurotoxicity by the Fractalkine Receptor. *Nat. Neurosci.* **2006**, *9*, 917–924.
34. Lee, S. M.; Yune, T. Y.; Kim, S. J.; Park, D. W.; Lee, Y. K.; Kim, Y. C.; Oh, Y. J.; Markelonis, G. J.; Oh, T. H. Minocycline Reduces Cell Death and Improves Functional Recovery after Traumatic Spinal Cord Injury in the Rat. *J. Neurotrauma* **2003**, *20*, 1017–1027.
35. Wells, J. E.; Hurlbert, R. J.; Fehlings, M. G.; Yong, V. W. Neuroprotection by Minocycline Facilitates Significant Recovery from Spinal Cord Injury in Mice. *Brain* **2003**, *126*, 1628–1637.
36. Teng, Y. D.; Choi, H.; Onario, R. C.; Zhu, S.; Desilets, F. C.; Lan, S.; Woodard, E. J.; Snyder, E. Y.; Eichler, M. E.; Friedlander, R. M. Minocycline Inhibits Contusion-Triggered Mitochondrial Cytochrome c Release and Mitigates Functional Deficits after Spinal Cord Injury. *Proc. Natl. Acad. Sci. U. S. A.* **2004**, *101*, 3071–3076.
37. Hains, B. C.; Waxman, S. G. Activated Microglia Contribute to the Maintenance of Chronic Pain after Spinal Cord Injury. *J. Neurosci.* **2006**, *26*, 4308–4317.
38. Garrido-Mesa, N.; Zarzuelo, A.; Galvez, J. Minocycline: Far beyond an Antibiotic. *Br. J. Pharmacol.* **2013**, *169*, 337–352.
39. Kremlev, S. G.; Roberts, R. L.; Palmer, C. Differential Expression of Chemokines and Chemokine Receptors during Microglial Activation and Inhibition. *J. Neuroimmunol.* **2004**, *149*, 1–9.
40. Cerqueira, S. R.; Oliveira, J. M.; Silva, N. A.; Leite-Almeida, H.; Ribeiro-Samy, S.; Almeida, A.; Mano, J. F.; Sousa, N.; Salgado, A. J.; Reis, R. L. Microglia Response and *In Vivo* Therapeutic Potential of Methylprednisolone-Loaded Dendrimer Nanoparticles in Spinal Cord Injury. *Small* **2013**, *9*, 738–749.
41. Tsoi, K. M.; Dai, Q.; Alman, B. A.; Chan, W. C. Are Quantum Dots Toxic? Exploring the Discrepancy between Cell Culture and Animal Studies. *Acc. Chem. Res.* **2013**, *46*, 662–671.
42. Dossi, M.; Ferrari, R.; Dragoni, L.; Martignoni, C.; Gaetani, P.; D'Incalci, M.; Morbidelli, M.; Moscatelli, D. Synthesis of Fluorescent PMMA-Based Nanoparticles. *Macromol. Mater. Eng.* **2013**, *298*, 771–778.
43. Cova, L.; Bigini, P.; Diana, V.; Sitia, L.; Ferrari, R.; Pesce, R. M.; Khalaf, R.; Bossolasco, P.; Ubezio, P.; Lupi, M.; *et al.* Biocompatible Fluorescent Nanoparticles for *In Vivo* Stem Cell Tracking. *Nanotechnology* **2013**, *24*, 245603.
44. De Paola, M.; Diana, V.; Bigini, P.; Mennini, T. Morphological Features and Responses to AMPA Receptor-Mediated Excitotoxicity of Mouse Motor Neurons: Comparison in Purified, Mixed Anterior Horn or Motor Neuron/Glia Cocultures. *J. Neurosci. Methods* **2008**, *170*, 85–95.
45. Ferrari, R.; Colombo, C.; Casali, C.; Lupi, M.; Ubezio, P.; Falcetta, F.; D'Incalci, M.; Morbidelli, M.; Moscatelli, D. Synthesis of Surfactant Free PCL-PEG Brushed Nanoparticles with Tunable Degradation Kinetics. *Int. J. Pharm.* **2013**, *453*, 551–559.